High-temperature superconductivity in a two-dimensional electride

Gui Wang [1], Pu Huang,[1] Zhengfang Qian,[1] Peng Zhang [1,*] and Su-Huai Wei[2]

[1]*Key Laboratory of Optoelectronic Devices and Systems of Ministry of Education and Guangdong Province,*
College of Physics and Optoelectronic Engineering, Shenzhen University, Shenzhen 518060, China
[2]*Beijing Computational Science Research Center, Beijing 100193, China*

Electrides constitute a unique class of materials that can be developed as conventional superconductors with diverse dimensional superconductivity. However, the transition temperatures (T_c) of electride superconductors are generally low and promoting their T_c usually requires extremely high external pressures that are formidable for practical applications. Here, based on the first-principles calculations, we proposed that the recently reported electride, Be_2N, can exhibit a two-dimensional (2D) superconductivity, which has a T_c of 10.3 K that is the highest T_c ever found for bulk electride superconductors at ambient pressure. More interestingly, we found that the high T_c of Be_2N is mainly attributed to the large average phonon frequency, rather than the strong electron-phonon coupling, which can be further understood by the small atomic weight of Be atoms and the strong Be-N bonds. Moreover, compared to most conventional superconductors, we identified an unusual dependence of the superconductivity of Be_2N on external pressures, originating from a unique charge transfer from its cationic framework to its anionic electron cloud. Our studies provide a deeper understanding of the superconductivity of 2D electrides and suggest a feasible way for the development of high-temperature electride superconductors at ambient pressure.

I. INTRODUCTION

Since the first discovery of Cs^+(15-crown-5)$2e^-$ by Dye and co-workers in 1982, electrides have attracted increasing research interest over the past four decades [1,2]. Unlike conventional ionic crystals, where both the positive and the negative constituents are ions, electrides consist of a cationic framework with excess electrons that locate in their structural cavities and serve as anions [3]. This unusual structural arrangement brings electrides exceptional physical properties, including high electrical conductivity and low work functions [4,5]. In particular, at low temperatures, superconducting transitions could also occur in electrides, as first demonstrated in $[Ca_{24}Al_{28}O_{64}]^{4+}(e^-)_4$ (C12A7 : e^-) [6]. Since then, a series of electride superconductors have been proposed, including Li_6P, Li_6C, Li_5Si, Li_5C, Ca_3Si, Li_3S, Nb_5Ir_3, and Zr_5Sb_3 [7–14]. Depending on their crystal structures, these electrides display diverse dimensional superconductivity and distinct superconducting behaviors, compared to the well-known high-pressure superconductors, such as H_3S [15], LaH_{10} [16], and YH_9 [17], which may open up a new avenue for the development of conventional superconductors.

The successful synthesis and identification of Ca_2N as the first two-dimensional (2D) electride in 2013 made alkaline-earth metal nitrides (AE_2N, AE = Be, Mg, Ca, Sr, Ba) an important family of electrides that have received extensive attention in recent years [4,18,19]. Inspired by their remarkable electronic transport properties, significant efforts have

also been paid to study the superconductivity of AE_2N. It has been reported that both Ca_2N and Ba_2N can exhibit 2D superconductivity at their monolayer limit and even the semiconducting Mg_2N transforms to a superconductor under external tensile strains [20–22]. However, the transition temperatures (T_c) of these AE_2N superconductors were predicted to be generally low, which was often ascribed to the weak electron-phonon coupling (EPC) in these materials. Moreover, for the bulk AE_2N at ambient pressure, superconductivity was still not reported. More recently, by careful symmetry analysis, we have proposed a ground-state structure for Be_2N, which is different from the anti-CdCl$_2$ structure of Ca_2N [23]. It has been shown that the width of the interlayer space in this Be_2N structure is only 1.43 Å, which is much smaller than the empirical values (3−5 Å) found for other AE_2N [23,24]. Thus, compared to other AE_2N, this structure character implies more concentrated anionic electrons and a much stronger interaction between these electrons and the cationic framework in Be_2N, which may together lead to the superconductivity with a promoted transition temperature.

To verify this anticipation, here we performed the first-principles calculations within the density functional perturbation theory (DFPT) method to systematically study the electronic and superconducting properties of Be_2N. Our results indicated that the exotic electronic structure of Be_2N drives it to be a 2D superconductor with a T_c of 10.3 K that is the highest T_c ever found for bulk electride superconductors at ambient pressure. More interestingly, different from the previous expectations, we identified that the high T_c of Be_2N is mainly attributed to its large average phonon frequency, rather than the strong EPC, which can be further understood by the

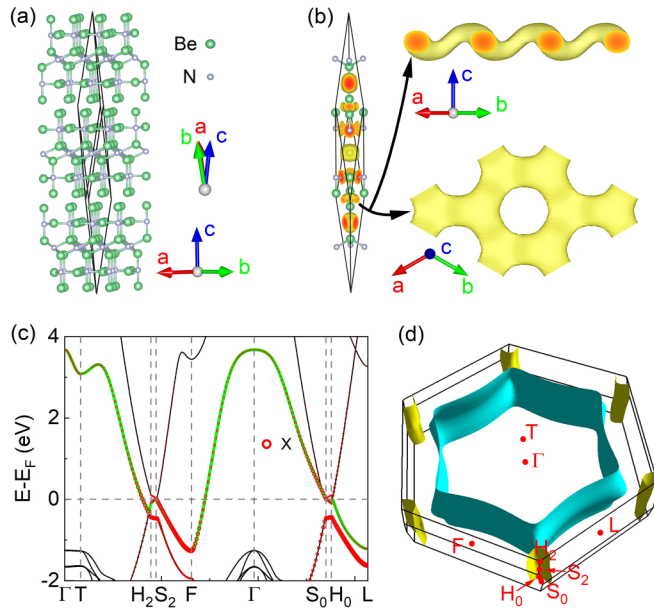*Corresponding author: pengzhang@szu.edu.cn

FIG. 1. (a) The crystal structure of Be_2N. (b) Three-dimensional (3D) and 2D plot of electron localization function (ELF) in Be_2N with the isosurface of 0.7. The 2D ELF is plotted for the top (001) surface of Be_2N with a $2 \times 2 \times 1$ supercell. (c) Projected band structure of Be_2N, where the contribution of anionic electrons is labeled as X and the metallic band across the Fermi level is highlighted by green. (d) 3D Fermi surface in Be_2N with the electron and hole pockets colored by cyan and yellow, respectively.

small atomic weight of Be atoms and the strong Be-N bonds. Moreover, the pressurization effect on the superconductivity of Be_2N was also considered. Compared to most conventional superconductors, our results indicated an unusual dependence of the superconducting behaviors of Be_2N on external pressures, which can be ascribed to a unique charge transfer from its cationic framework to its anionic electron cloud.

II. COMPUTATIONAL METHODS

The first-principles calculations were carried out by using the projector augmented wave method based on the density functional theory as implemented in the QUANTUM ESPRESSO (QE) code [25]. The exchange-correlation energy was treated by the generalized gradient approximation method with the Perdew-Burke-Ernzerhof functional [26]. The SG15 optimized norm-conserving Vanderbilt pseudopotentials [27] were employed to describe the effect of core electrons, and the energy cutoffs of 80 and 320 Ry were chosen for the wave functions and the charge densities, respectively. The Fermi

surface was broadened by the Gaussian smearing method [28] with a width of 0.008 Ry, and the van der Waals correction adopts the rVV10 approach [29]. The EPC constants were calculated based on the DFPT [30] with a $4 \times 4 \times 4$ q-point grid and a $16 \times 16 \times 16$ k-point grid, and the T_c was estimated by using the McMillan-Allen-Dynes formula [31]. The crystal orbital Hamilton population [32] curves are obtained using the LOBSTER code [33].

III. RESULTS AND DISCUSSION

As reported previously, the ground-state structure of Be_2N possesses a layered framework with the $R\bar{3}m$ symmetry, as illustrated in Fig. 1(a) (the detailed structural information is given in the Supplemental Material [34]). Here, the lattice parameters of Be_2N were calculated to be $a = b = 2.841$ Å and $c = 28.603$ Å by QE, which is in good agreement with that calculated by VASP [23] (see Supplemental Material Table S1 [34]). The anionic electrons in Be_2N were found to locate mainly in the interlayer space between adjacent [Be_2N] slabs, forming a 2D electron gas in the ab plane, as shown in Fig. 1(b). Thus, similar to Ca_2N, Be_2N is also a 2D electride, despite their different crystal structures. The width of the interlayer space in Be_2N was calculated to be 1.43 Å, which is much smaller than that reported for other AE_2N, such as Ca_2N (3.90 Å), Sr_2N (4.24 Å), and Ba_2N (4.54 Å) [23]. Consequently, Be_2N has a much higher density of anionic electrons than other AE_2N, as shown in Table I, which is beneficial to improve the electrical conductivity and realize the superconductivity in Be_2N.

Figure 1(c) plots the projected band structure of Be_2N. It is clear to see that Be_2N is a metal with only one band (green) crossing the Fermi level (E_F). A detailed inspection of this metallic band indicated that it is mainly contributed by the anionic electrons, with only a small hybridization with Be $2s$ and N $2p$ orbitals (see Fig. S1 [34]). The corresponding Fermi surface for this metallic band is shown in Fig. 1(d), which illustrates a hexagonal toroidal electron pocket at the center of the first Brillouin zone (FBZ) and a triangular tubelike hole pocket at each corner. These results implied that the electronic transport properties of Be_2N should largely rely on its anionic electrons. Moreover, from Fig. 1(c), we can also see that the metallic band is highly dispersive along the T-H_2, F-Γ, and Γ-S_0 high-symmetry lines but becomes relatively flat along the H_2-S_2 and S_0-H_0 high-symmetry lines around E_F. The coexistence of these steep and flat bands near E_F would provide a vanishing Fermi velocity to part of the conduction electrons, which is favorable for the formation of Cooper pairs and thus essential to realize the superconductivity in electride superconductors [35–37].

TABLE I. The number of anionic electrons, λ, $\omega_{\log}$, average bond length, and integrated COHP (ICOHP) in Be_2N, as well as that in Ca_2N and Ba_2N monolayers.

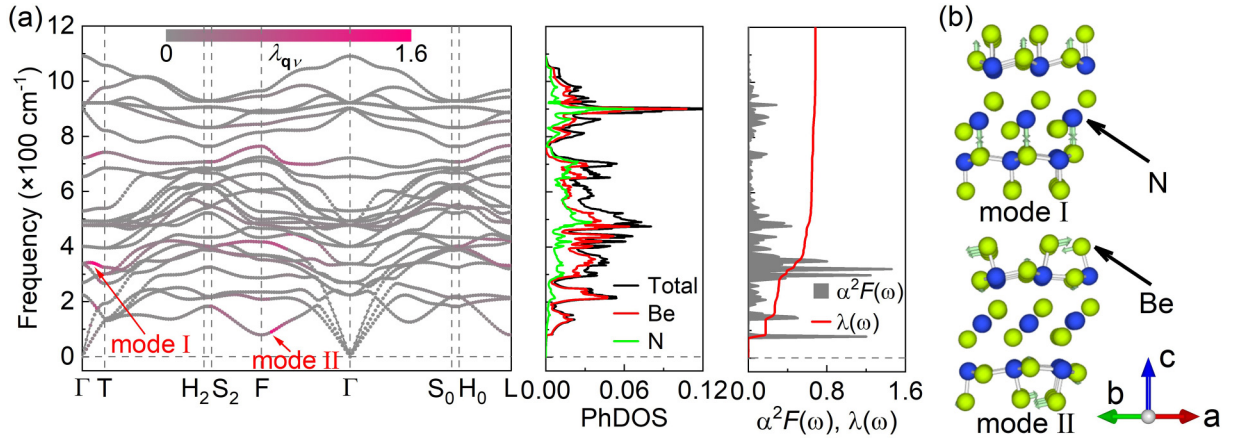| AE_2N	Structure	Anionic electron (e^-/f.u.)	λ	$\omega_{\log}$ (K)	Bond length (Å)	−ICOHP
Be_2N	bulk	0.127	0.68	314	1.705	1.32
Ca_2N [20]	monolayer	0.038	0.78	158	2.417	0.44
Ba_2N [21]	monolayer	0.020	0.59	103	2.767	0.29

FIG. 2. (a) Phonon spectrum with the projected EPC constants ($\lambda_{\mathbf{q}\nu}$), PhDOS, Eliashberg function [$\alpha^2 F(\omega)$], and integrated EPC constant [$\lambda(\omega)$] for Be$_2$N. (b) Vibrational patterns for mode I and mode II, where aqua arrows represent the direction of atomic vibration.

To estimate the superconductivity of Be$_2$N, the corresponding EPC parameters [$\lambda_{\mathbf{q}\nu}$, $\alpha^2 F(\omega)$, λ] were calculated. Among them, λ can be estimated either by summing the projected EPC constant ($\lambda_{\mathbf{q}\nu}$) for all phonon modes in the whole FBZ or by integrating the Eliashberg spectral function [$\alpha^2 F(\omega)$] as follows:

$$\lambda = \sum_{\mathbf{q}\nu} \lambda_{\mathbf{q}\nu} = 2 \int \frac{\alpha^2 F(\omega)}{\omega} d\omega, \qquad (1)$$

where ω is the phonon frequency, $\lambda_{\mathbf{q}\nu}$ was calculated by

$$\lambda_{\mathbf{q}\nu} = \frac{\gamma_{\mathbf{q}\nu}}{\pi \hbar N(E_F) \omega_{\mathbf{q}\nu}^2}, \qquad (2)$$

and $\alpha^2 F(\omega)$ was calculated by

$$\alpha^2 F(\omega) = \frac{1}{2\pi N(E_F)} \sum_{\mathbf{q}\nu} \delta(\omega - \omega_{\mathbf{q}\nu}) \frac{\gamma_{\mathbf{q}\nu}}{\hbar \omega_{\mathbf{q}\nu}}, \qquad (3)$$

$$\gamma_{\mathbf{q}\nu} = 2\pi \omega_{\mathbf{q}\nu} \sum_{ij} \int \frac{d\mathbf{k}}{\Omega_{BZ}} |g_{\mathbf{q}\nu}(\mathbf{k}, i, j)|^2$$
$$\times \delta(\epsilon_{\mathbf{k},i} - E_F) \delta(\epsilon_{\mathbf{k}+\mathbf{q},j} - E_F), \qquad (4)$$

where $N(E_F)$ is the electronic density of states at E_F, $\gamma_{\mathbf{q}\nu}$ presents the phonon linewidth, and $g_{\mathbf{q}\nu}$ denotes the EPC matrix element.

Figure 2(a) shows the calculated phonon spectrum, phonon density of states (PhDOS), and EPC parameters for Be$_2$N. There are totally 27 phonon branches, including 3 acoustic and 24 optical branches, respectively. λ was calculated to be 0.68 for Be$_2$N, which is comparable to that found for Ca$_2$N and Ba$_2$N monolayers, as given in Table I. From $\alpha^2 F(\omega)$, we identified that the most significant contribution to λ comes from the phonon modes within the frequency range from 80 to 120 cm^{-1} and that from 250 to 350 cm^{-1}. Moreover, the phonon modes that have the largest $\lambda_{\mathbf{q}\nu}$ were found to be along the Γ-T (mode I) and F-Γ (mode II) high-symmetry lines, with the frequencies of 338 and 90 cm^{-1}, respectively. The real-space atomic vibrational patterns indicated that both these phonon modes are largely dominated by the vibration of Be atoms, as shown in Fig. 2(b). Consistent results were also obtained in PhDOS, where the Be contribution dominates the low-frequency range from 0 to 500 cm^{-1}. From these

calculations, we can deduce that it is the coupling between the Be vibration and anionic electrons that determines the superconductivity of Be$_2$N.

The T_c of Be$_2$N was estimated by the McMillan-Allen-Dynes formula [31],

$$T_c = \frac{\omega_{\log}}{1.2} \exp\left(-\frac{1.04(1+\lambda)}{\lambda - (1 + 0.62\lambda)\mu^*}\right), \qquad (5)$$

$$\omega_{\log} = \exp\left(\frac{2}{\lambda} \int \frac{\alpha^2 F(\omega) \ln \omega}{\omega} d\omega\right), \qquad (6)$$

where $\omega_{\log}$ and μ^* denote the logarithmically averaged characteristic phonon frequency and the Coulomb pseudopotential that typically has a system-independent value, respectively. Here, we adopted a typical value of 0.1 for μ^* [40,41]. Interestingly, our calculations showed that the T_c of Be$_2$N can reach 10.3 K at ambient pressure, which is more than two and three times larger than that of Ca$_2$N and Ba$_2$N monolayers, respectively, as shown in Table I. Moreover, by surveying all the reported bulk electride superconductors at ambient pressure, we identified that Be$_2$N still has the highest T_c, as shown in Table II. Obviously, this high T_c of Be$_2$N cannot be attributed to the strong EPC, since it has only a moderate λ that is even smaller than that found for Ca$_2$N monolayer. On the other hand, we found that Be$_2$N has a much larger

TABLE II. Crystal structures and transition temperatures (T_c) of electride superconductors at ambient pressure.

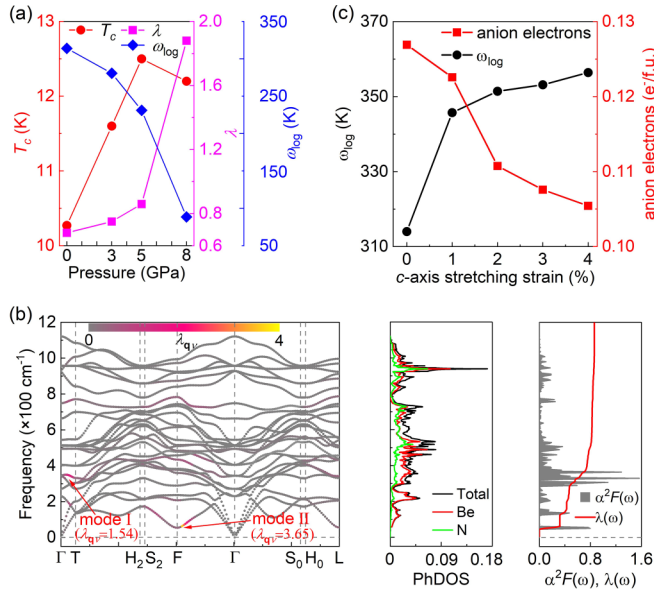| Formula	Symmetry	Bulk or monolayer	T_c/K	Ref.
Be$_2$N	$R\bar{3}m$	Bulk	10.3	Our work
Mg$_2$N	$R3m$	Bulk	0.3	[22]
Ca$_2$N	$R\bar{3}m$	Monolayer	4.7	[20]
Ba$_2$N	$R\bar{3}m$	Monolayer	3.4	[21]
Y$_2$C	$R\bar{3}m$	Monolayer	0.9	[38]
MgONa		Monolayer	3.4	[38]
C12A7 : e^-	$I\bar{4}3d$	Bulk	~0.4 (Expt.)	[6]
Nb$_5$Ir$_3$	$P6_3/mcm$	Bulk	9.4 (Expt.)	[13]
Zr$_5$Sb$_3$	$P6_3/mcm$	Bulk	~2.3 (Expt.)	[14]
Li$_5$Si	$P6/mmm$	Bulk	1.1	[9]
AlH$_2$	$P\bar{6}m2$	Monolayer	38	[39]

FIG. 3. (a) The T_c, λ, and $\omega_{\log}$ of Be$_2$N calculated at different pressures. (b) Phonon spectrum with $\lambda_{\mathbf{q}\nu}$, PhDOS, $\alpha^2 F(\omega)$, and $\lambda(\omega)$ for Be$_2$N at 5 GPa. (c) The $\omega_{\log}$ and number of anion electrons in Be$_2$N calculated at various c-axis stretching strains. The number of anion electrons was calculated according to the Bader charge [42].

$\omega_{\log}$ than that of Ca$_2$N and Ba$_2$N monolayers, which should be mainly responsible for its high T_c, as shown in Table I. Since the Be vibration dominates the low-frequency phonon spectrum of Be$_2$N, this large $\omega_{\log}$ can be partly understood by the small atomic weight of Be atoms, which tends to facilitate the atomic vibration. In addition, compared to Ca$_2$N and Ba$_2$N monolayers, we found that Be$_2$N possesses much stronger chemical bonds, as shown in Table I. These strong Be-N bonds and the corresponding robust crystal lattice of Be$_2$N would also prefer to enlarge its phonon frequencies.

It has been widely recognized that pressurization usually plays an effective role in enhancing the T_c of conventional superconductors. Accordingly, here we also studied its effect on the superconductivity of Be$_2$N. Figure 3(a) plots the variation of T_c, λ, and $\omega_{\log}$ for Be$_2$N, as the pressure changes from 0 to 8 GPa. Moreover, to check its structural stability at high pressures, we performed the ground-state structure search for Be$_2$N at 10 GPa with the CALYPSO code [43,44] and the results indicated that its ground-state structure does not change after searching for 30 generations with 900 structures (see Fig. S2 [34]). As shown in Fig. 3(a), λ was found to increase monotonically as the pressure increases from 0 to 8 GPa, suggesting a continuously enhanced EPC in Be$_2$N. Similar results can also be obtained in Fig. 3(b), where $\lambda_{\mathbf{q}\nu}$ for model I and model II calculated at 5 GPa are significantly larger than that calculated at 0 GPa, which leads to an enhanced λ of 0.82 and a promoted T_c of 12.5 K at 5 GPa. However, on the other hand, it is surprising to see that $\omega_{\log}$ of Be$_2$N decreases monotonically in the same pressure range, contrary to the common trend found for most conventional superconductors [7,45,46]. Consequently, the T_c does not continue to increase but decreases to 12.2 K, as the pressure increases

from 5 to 8 GPa, which illustrates that the pressurization cannot effectively enhance the T_c of Be$_2$N. To understand this unexpected decrease of $\omega_{\log}$, we examined the change of anionic electrons in Be$_2$N, as the pressure increases from 0 to 5 GPa. The results showed a 4.2% increase of the number of anionic electrons in Be$_2$N at 5 GPa, compared to that at 0 GPa, indicating a charge transfer from [Be$_2$N] slabs to the anionic electron cloud. This depletion of charge from [Be$_2$N] slabs would weaken the Be-N bonds and consequently reduce $\omega_{\log}$ of Be$_2$N. For comparison, we also examined the anionic electron change in Be$_2$N under different stretching strains along the c direction. As expected, a reversed charge transfer from the anionic electron cloud to [Be$_2$N] slabs was found, resulting in an increased $\omega_{\log}$, as shown in Fig. 3(c). These results elucidated that, different from most conventional superconductors, the existence of anionic electrons may endow distinct superconducting behaviors to electride superconductors.

IV. CONCLUSIONS

In summary, based on the first-principles calculations, we have studied the electronic and superconducting properties of a recently proposed 2D electride, Be$_2$N. Our results indicated that the exotic electronic structure of Be$_2$N drives it to be a 2D superconductor with a T_c of 10.3 K that is the highest T_c ever found for bulk electride superconductors at ambient pressure. More interestingly, we uncovered that this high T_c of Be$_2$N is mainly attributed to the large average phonon frequency, rather than the strong EPC, which can be further understood by the small atomic weight of Be atoms and the strong Be-N bonds. Moreover, the calculations also revealed that pressurization has an unusual effect on the superconducting behaviors of Be$_2$N, deviating from the general trend found for most conventional superconductors. This phenomenon can be understood by a unique charge transfer from the cationic framework to the anionic electron cloud in Be$_2$N, which tends to weaken the Be-N bonds and thus reduce its average phonon frequency. Our studies thus deepen the understanding of the superconductivity of 2D electrides and meanwhile suggest a possible way to enhance the T_c of electride superconductors at ambient pressure.

[1] L. D. Le, D. Issa, B. Van Eck, and J. L. Dye, J. Phys. Chem. **86**, 7 (1982).

[2] H. Hosono and M. Kitano, Chem. Rev. **121**, 3121 (2021).

[3] S. Matsuishi, Y. Toda, M. Miyakawa, K. Hayashi, T. Kamiya, M. Hirano, I. Tanaka, and H. Hosono, Science **301**, 626 (2003).

[4] K. Lee, S. W. Kim, Y. Toda, S. Matsuishi, and H. Hosono, Nature (London) **494**, 336 (2013).

[5] Y. Toda, H. Yanagi, E. Ikenaga, J. J. Kim, M. Kobata, S. Ueda, T. Kamiya, M. Hirano, K. Kobayashi, and H. Hosono, Adv. Mater. **19**, 3564 (2007).

[6] M. Miyakawa, S. W. Kim, M. Hirano, Y. Kohama, H. Kawaji, T. Atake, H. Ikegami, K. Kono, and H. Hosono, J. Am. Chem. Soc. **129**, 7270 (2007).

[7] Z. Zhao, S. Zhang, T. Yu, H. Xu, A. Bergara, and G. Yang, Phys. Rev. Lett. **122**, 097002 (2019).

[8] Z. Liu, Q. Zhuang, F. Tian, D. Duan, H. Song, Z. Zhang, F. Li, H. Li, D. Li, and T. Cui, Phys. Rev. Lett. **127**, 157002 (2021).

[9] J. You, B. Gu, G. Su, and Y. P. Feng, J. Am. Chem. Soc. **144**, 5527 (2022).

[10] Z. S. Pereira, G. M. Faccin, and E. Z. Da Silva, J. Phys. Chem. C **125**, 8899 (2021).

[11] B. Sa, R. Xiong, C. Wen, Y. Li, P. Lin, Q. Lin, M. Anpo, and Z. Sun, J. Phys. Chem. C **124**, 7683 (2020).

[12] C. Kokail, C. Heil, and L. Boeri, Phys. Rev. B **94**, 060502(R) (2016).

[13] Y. Zhang, B. Wang, Z. Xiao, Y. Lu, T. Kamiya, Y. Uwatoko, H. Kageyama, and H. Hosono, npj Quantum Mater. **2**, 45 (2017).

[14] B. Lv, X. Y. Zhu, B. Lorenz, F. Y. Wei, Y. Y. Xue, Z. P. Yin, G. Kotliar, and C. W. Chu, Phys. Rev. B **88**, 134520 (2013).

[15] A. P. Drozdov, M. I. Eremets, I. A. Troyan, V. Ksenofontov, and S. I. Shylin, Nature (London) **525**, 73 (2015).

[16] A. P. Drozdov, P. P. Kong, V. S. Minkov, S. P. Besedin, M. A. Kuzovnikov, S. Mozaffari, L. Balicas, F. F. Balakirev, D. E. Graf, V. B. Prakapenka, E. Greenberg, D. A. Knyazev, M. Tkacz, and M. I. Eremets, Nature (London) **569**, 528 (2019).

[17] F. Peng, Y. Sun, C. J. Pickard, R. J. Needs, Q. Wu, and Y. Ma, Phys. Rev. Lett. **119**, 107001 (2017).

[18] J. S. Oh, C. Kang, Y. J. Kim, S. Sinn, M. Han, Y. J. Chang, B. Park, S. W. Kim, B. I. Min, H. Kim, and T. W. Noh, J. Am. Chem. Soc. **138**, 2496 (2016).

[19] D. L. Druffel, K. L. Kuntz, A. H. Woomer, F. M. Alcorn, J. Hu, C. L. Donley, and S. C. Warren, J. Am. Chem. Soc. **138**, 16089 (2016).

[20] X. Zeng, S. Zhao, Z. Li, and J. Yang, Phys. Rev. B **98**, 155443 (2018).

[21] X. L. Qiu, J. F. Zhang, H. C. Yang, Z. Y. Lu, and K. Liu, Phys. Rev. B **105**, 165101 (2022).

[22] G. Wang, Y. Zhong, Y. Xu, Z. Qian, J. Jiang, and Z. Ma, Phys. Chem. Chem. Phys. **25**, 17300 (2023).

[23] G. Wang, Z. Ma, J. W. Jiang, J. K. Yang, Y. L. Sun, Z. F. Qian, P. Huang, P. Zhang, and S. H. Wei, Phys. Rev. Appl. **19**, 034014 (2023).

[24] T. Inoshita, S. Jeong, N. Hamada, and H. Hosono, Phys. Rev. X **4**, 031023 (2014).

[25] P. Giannozzi, S. Baroni, N. Bonini, M. Calandra, R. Car, C. Cavazzoni, D. Ceresoli, G. L. Chiarotti, M. Cococcioni, I. Dabo, A. Dal Corso, S. de Gironcoli, S. Fabris, G. Fratesi, R. Gebauer, U. Gerstmann, C. Gougoussis, A. Kokalj, M. Lazzeri, L. Martin-Samos, N. Marzari, F. Mauri, R. Mazzarello, S. Paolini, A. Pasquarello, L. Paulatto, C. Sbraccia, S. Scandolo, G. Sclauzero, A. P. Seitsonen, A. Smogunov, P. Umari, and R. M. Wentzcovitch, J. Phys.: Condens. Matter **21**, 395502 (2009).

[26] J. P. Perdew, K. Burke, and M. Ernzerhof, Phys. Rev. Lett. **77**, 3865 (1996).

[27] D. R. Hamann, Phys. Rev. B **88**, 085117 (2013).

[28] N. Marzari, D. Vanderbilt, A. De Vita, and M. C. Payne, Phys. Rev. Lett. **82**, 3296 (1999).

[29] R. Sabatini, T. Gorni, and S. de Gironcoli, Phys. Rev. B **87**, 041108(R) (2013).

[30] S. Baroni, S. de Gironcoli, A. Dal Corso, and P. Giannozzi, Rev. Mod. Phys. **73**, 515 (2001).

[31] P. B. Allen and R. C. Dynes, Phys. Rev. B **12**, 905 (1975).

[32] R. Dronskowski and P. E. Bloechl, J. Phys. Chem. **97**, 8617 (1993).

[33] R. Nelson, C. Ertural, J. George, V. L. Deringer, G. Hautier, and R. Dronskowski, J. Comput. Chem. **41**, 1931 (2020).

[34] See Supplemental Material at http://link.aps.org/supplemental/10.1103/PhysRevB.109.014504 for structural information, electronic structures, CALYPSO searching, and phonon dispersion curves of Be$_2$N electride, which includes Refs. [23,43,44].

[35] H. J. Choi, D. Roundy, H. Sun, M. L. Cohen, and S. G. Louie, Nature (London) **418**, 758 (2002).

[36] A. Simon, Angew. Chem., Int. Ed. Engl. **36**, 1788 (1997).

[37] J. Hou, X. Dong, A. R. Oganov, X. J. Weng, C. M. Hao, G. Yang, H. T. Wang, X. F. Zhou, and Y. Tian, Phys. Rev. B **106**, L220501 (2022).

[38] Y. Ge, S. Guan, and Y. Liu, New J. Phys. **19**, 123020 (2017).

[39] Q. Yang, X. Jiang, and J. Zhao, Chin. Phys. Lett. **40**, 107401 (2023).

[40] T. T. Pham and D. L. Nguyen, Phys. Rev. B **107**, 134502 (2023).

[41] W. Sun, B. Chen, X. Li, F. Peng, A. Hermann, and C. Lu, Phys. Rev. B **107**, 214511 (2023).

[42] W. Tang, E. Sanville, and G. Henkelman, J. Phys.: Condens. Matter **21**, 84204 (2009).

[43] Y. Wang, J. Lv, L. Zhu, and Y. Ma, Phys. Rev. B **82**, 094116 (2010).

[44] Y. Wang, J. Lv, L. Zhu, and Y. Ma, Comput. Phys. Commun. **183**, 2063 (2012).

[45] X. L. He, P. Zhang, Y. Ma, H. Li, X. Zhong, Y. Wang, H. Liu, and Y. Ma, Phys. Rev. B **107**, 134509 (2023).

[46] Q. Wang, K. Zhao, S. Wei, H. Liu, and S. Zhang, Mater. Today Phys. **28**, 100853 (2022).